ELSEVIER

Journal of Nuclear Materials 258–263 (1998) 945–949

journal of nuclear materials

Section 5.4. High heat flux materials (Cu, refractory metals)

Microstructural evolution in Cu–A125 alloy under 300 keV Cu^+ ion irradiation

Jing Li [a,b,*], Hui Xu [a,b], Jinnan Yu [c], Baoli Wu [a,b], Qingfu He [d]

[a] *Beijing Research Institute of Materials and Technology, P.O. Box 9211, Beijing 100076, People's Republic of China*
[b] *Beijing Laboratory of Electron Microscopy, Chinese Academy of Sciences, P.O. Box 2724, Beijing 100080, People's Republic of China*
[c] *China Institute of Atomic Energy, P.O. Box 275-51, Beijing 102413, People's Republic of China*
[d] *Department of Mechanical Engineering, Northern Jiaotong University, Beijing 100044, People's Republic of China*

Abstract

Dispersion strengthened (DS) Cu–Al25 alloy containing small Al_2O_3 particles (~4 nm in diameter) was irradiated by 300 keV Cu^+ ion to doses of 10 dpa and 30 dpa with a displacement rate of 3.7×10^{-2} dpa/s at room temperature, which simulates the effects of high energy primary knock-on atoms (PKA) produced by 14 MeV neutrons. Microstructural evolution was investigated by transmission electron microscopy (TEM). Selected area diffraction (SAD) was used to study the phase stability of alumina under irradiation. The defect cluster structure formed by irradiation was investigated by dynamic two-beam techniques. Small particles of Al_2O_3 were dissolved under ion irradiation with increasing fluences. A large number of small Frank vacancy and interstitial dislocation loops (~5 nm in diameter) with different Burgers vectors of $a/3\langle 1\,1\,1\rangle$ are produced by ion irradiation. At the region adjacent to the irradiation surface the number of vacancy loops was greater than that of interstitial ones. This result is in good agreement with the computer simulation results.

1. Introduction

Dispersion strengthened (DS) high strength, high conductivity Cu–Al_2O_3 alloys have been considered as a candidate high heat flux alloy for fusion applications. Radiation effects on the microstructural evolution in this alloy have been studied by many authors [1–7]. Most of these investigations were focused on the phase stability of Al_2O_3 particles under irradiation. There is a little data on defect cluster structures from cascade damage in this alloy. In this study a Cu–Al25 alloy, with very small (~4 nm in diameter) Al_2O_3 particles, was irradiated by 300 keV Cu^+ ion to simulate the effects of high energy primary knock-on atoms (PKA) produced by 14 MeV neutrons. The phase stability of Al_2O_3 particles and defect cluster structures (Frank dislocation loops) induced by ion irradiation was investigated by transmission electron microscopy (TEM).

2. Experimental procedure

The material for this investigation was Glidcop Al-25 which will be used in the ITER structural material, a Cu–Al_2O_3 DS alloy containing 0.25 wt% Al in the form of Al_2O_3 particles (~4 nm in diameter), see Fig. 1. TEM disks of dimensions ϕ 3 mm × 50 μm were pre-electrochemically thinned using a twin-jet polishing unit in an electrolyte of 0.33% nitric acid in methanol at a temperature of −20°C and a voltage of 25 V.

The specimens were then irradiated with 300 keV Cu^+ ions at a displacement rate of 3.7×10^{-2} dpa/s (displacements per atom per second) to doses of 10 dpa and 30 dpa at room temperature. After irradiation, the specimens were thinned for a short time (about one hour) from the unirradiated side by an ion milling machine until perforation. The unirradiated samples were prepared using the same method. No observable damage was created by the ion milling procedure, see Fig. 1.

TEM observation was performed using a Hitachi H-700H electron microscope operated at 200 kV and a Philips EM 420 microscope operated at 100 kV. The

* Corresponding author. Tel.: +86 10 6838 3580; fax: +86 10 6838 3237; e-mail: jzhang@netchina.com.cn.

0022-3115/98/$19.00
PII: S0022-3115(98)00387-0

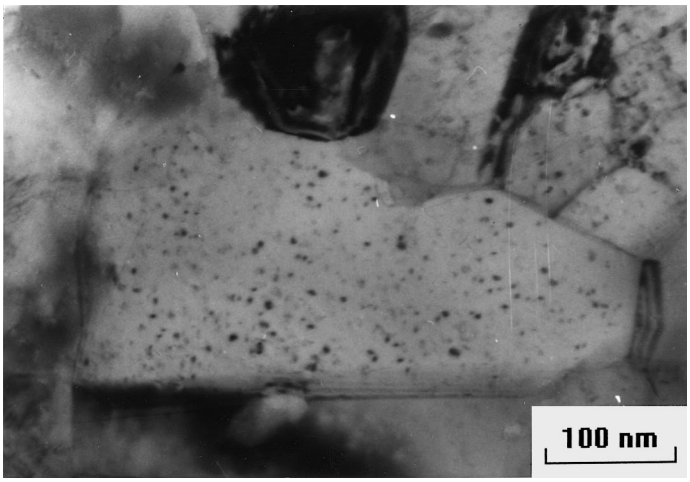

Fig. 1. BF TEM micrograph of unirradiated Cu–Al25 alloy showing a uniform distribution of small alumina particles (~4 nm in diameter). No damage was introduced by TEM sample preparation.

Al_2O_3 phase was determined by selected area diffraction (SAD). A precipitate diffraction ring with a interplanar spacing of 0.24 nm corresponds to the {3 1 1} interplanar spacing for γ-Al_2O_3. The "relative intensity" of this ring before and after irradiation was observed to study phase stability of alumina under ion irradiation. The defects produced by irradiation were observed under dynamic two-beam conditions for different foil orientations and different reflection vectors $\vec{g}$. The irradiation surface always faced into the electron beam for TEM observation.

A method, which was developed by many authors [8–14] to study small Frank loops with a diameter smaller as 0.2 ξ_g (ξ_g: extinction distance), that is: ~5 nm, was used in this investigation.

The distribution of ions and vacancies produced by 300 keV Cu^+ ions was calculated by the TRIM code. The damage dose rate is determined by the product of ion flux and damage rate per ion.

3. Results

Fig. 1 shows a typical bright field (BF) TEM micrograph of dispersed Al_2O_3 in Cu–Al25 prior to irradiation. Fig. 2(a) shows the SAD pattern; the {3 1 1} diffraction ring of Al_2O_3 is visible. Fig. 2(b) and (c) show the SAD patterns of Cu–Al25 after irradiation. The intensity of the {3 1 1} ring after irradiation to 10 dpa decreases considerably in comparison with the state before irradiation (Fig. 2(b)). Only a very weak {3 1 1} ring was observed for the irradiated specimens with 30 dpa (Fig. 2(c)). This indicated that Al_2O_3 particles were dissolved under ion irradiation with increasing fluences.

Fig. 3(a, b) show the typical TEM micrograph of Cu–Al25 alloy irradiated to 10 dpa and 30 dpa. The high density of black/white contrast lobes (BW lobes) is visible, showing the typical contrast of small Frank dislocation loops. A detailed investigation has been made following the literature [8–14] to characterize these Frank loops.

By defining a vector $\vec{l}$ as joining the black to the white lobe, the main features of BW lobes observed by this study are summarized as follows:

- For different dynamic images obtained with different $\vec{g}$ and different foil orientations, the directions of $\vec{l}$ were usually approximately within $\pm 10^\circ$ parallel to the projected $\langle 1\,1\,1 \rangle$ habit plane normals, independent of the operative reflection and foil orientation of the same grain.
- BW lobes with opposite $\vec{l}$ directions were frequently observed in TEM micrographs (Fig. 4).
- In many cases, with BF and dark field (DF) TEM dynamic images, the $\vec{l}$ direction of BW lobes which lie in the same position in BF and DF images is identical. This means that the loops observed under dynamic two-beam conditions lie near the top of the foil [8,9,12,13], that is, a region adjacent to the irradiation surface. Following a detailed analysis it is suggested that most of the loops, which have good imaged black/white lobe contrast, lie within ~10 nm (about 0.35 ξ_g for general two-beam conditions in Cu) of the surface, that is: lie in the layer 1 of the BF image [13].
- A statistical analysis for sign of $(\mathbf{g} \cdot \mathbf{l})$ has been performed and the result indicated: for many different grains and different two-beam conditions, the events for $(\mathbf{g} \cdot \mathbf{l}) > 0$ are much more than ones for $(\mathbf{g} \cdot \mathbf{l}) < 0$.

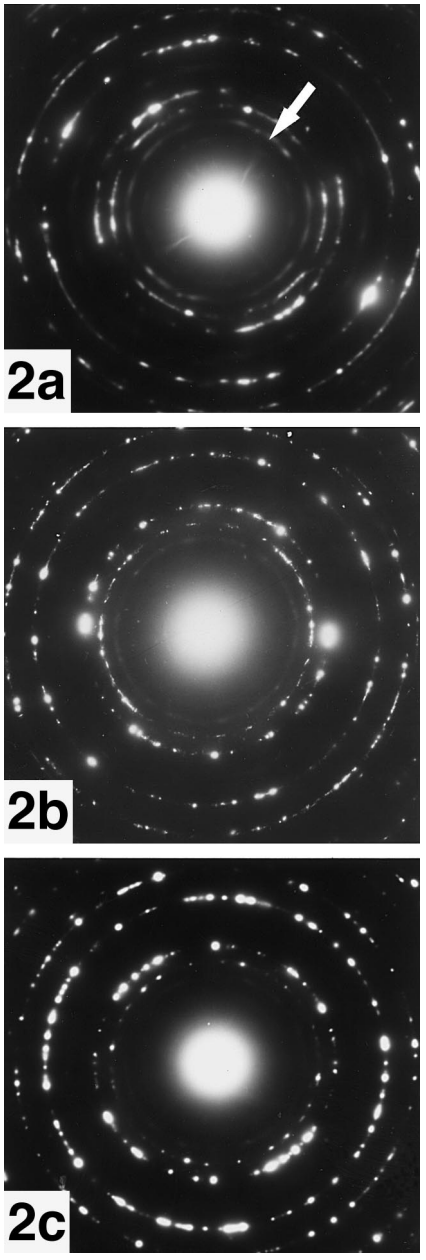

Fig. 2. SAD patterns of Cu–Al25 alloy: (a) typical SAD pattern of unirradiated specimen. The ring indicated by the arrow corresponds to a d-spacing of 0.24 nm, a {3 1 1} interplanar spacing for γ-Al_2O_3. (b) SAD pattern after irradiation to 10 dpa. The intensity of the {3 1 1} ring of Al_2O_3 decreases considerably. (c) SAD pattern after irradiation to 30 dpa. The {3 1 1} ring of Al_2O_3 becomes very weak.

According to the above described characteristics of BW lobes, the nature of the Frank loops can be identified as follows: (i) These Frank loops have different Burgers vectors of a/3 ⟨1 1 1⟩; (ii) Both vacancy and interstitial dislocation loops were observed; (iii) At the region adjacent to the irradiation surface, the number of vacancy loops are more than that of interstitial ones.

4. Discussion

4.1. Phase stability of alumina

300 keV Cu^+ ion irradiation can simulate the effects of high energy PKA produced by 14 MeV neutron. The results indicated that small Al_2O_3 particles can be dissolved by the cascades of high energy PKA. This is essentially in agreement with the results of other authors [5,7]. The dissolution of Al_2O_3 particles observed in this work is more remarkable than that in other works [5,7]. The reason is that the size of Al_2O_3 particles in these specimens is smaller ($\sim$4 nm) than that in other works ($\sim$10 nm), therefore they were most strongly affected by recoil resolution [7].

4.2. Formation of Frank loops under ion irradiation

Incident Cu^+ ions with 300 keV energy are able to produce cascades and subcascades. Within the cascade zones a large number of point defects and defect clusters are produced. The defect clusters can form the nucleus of vacancy and interstitial loops, which will grow vacancy and interstitial dislocation loops by the migration and accumulation of point defects. The incident Cu^+ ions can also form interstitial atoms and enhance the formation of interstitial loops.

In the cascade zones a part of the recoil atoms can be ejected far apart from this region by the collision sequence, and the cascade becomes a depleted zone [15]. If the vacancy concentration in the matrix is high enough, the depleted zone will evolve to a vacancy dislocation loop. Fig. 5 shows the vacancy and incident ion distribution along the depth in the specimen irradiated by 300 KeV Cu^+ ions as calculated with the TRIM code. It is shown that the peak values for vacancies and incident ions are near 50 nm and 100 nm in depth, respectively. This means that at the region adjacent to the irradiation surface layer the number of vacancy loops is more than that of interstitial ones, whereas in the deep layer the number of interstitial loops is higher than that of the vacancy loops. The experimental observations are in good agreement with the above mentioned predictions.

The group of BW lobes observed by TEM (Fig. 3(a,b)) implies a loop group, which consists of some Frank loops which lie very close each other and have the same Burgers vector. It seems that a set of subcascades had formed.

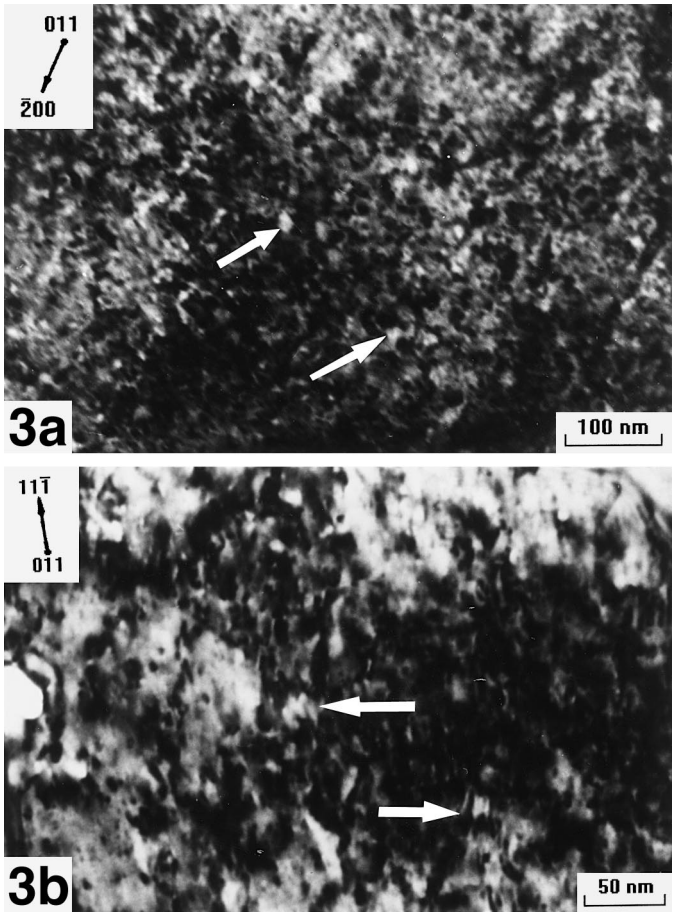

Fig. 3. Dynamic BF TEM micrograph of Cu–Al25 alloy showing typical microstructure after irradiation (a) to 10 dpa, foil plane = (0 1 1), $\vec{g} = [\bar{2}\,0\,0]$; (b) to 30 dpa, foil plane = (0 1 1), $\vec{g} = [1\,1\,\bar{1}]$. The high density of BW lobes with various $\vec{l}$ directions is visible. The arrows show the group of BW lobes.

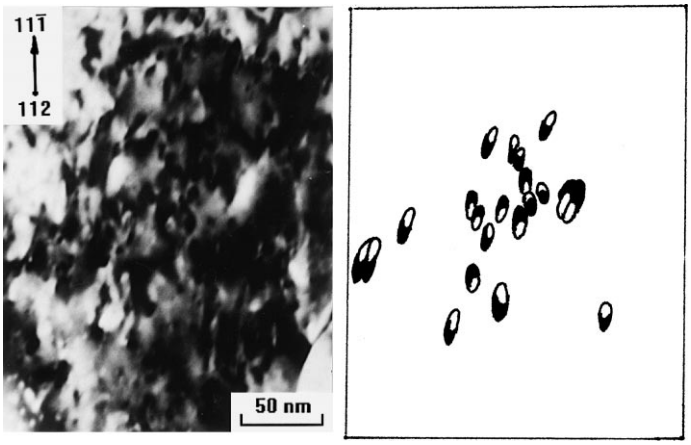

Fig. 4. BW lobes with opposite $\vec{l}$ directions show that ion irradiation produced both vacancy and interstitial Frank loops in Cu–Al25 alloy. Foil plane = (1 1 2), $\vec{g} = [1\,1\,\bar{1}]$. Damage level: 10 dpa.

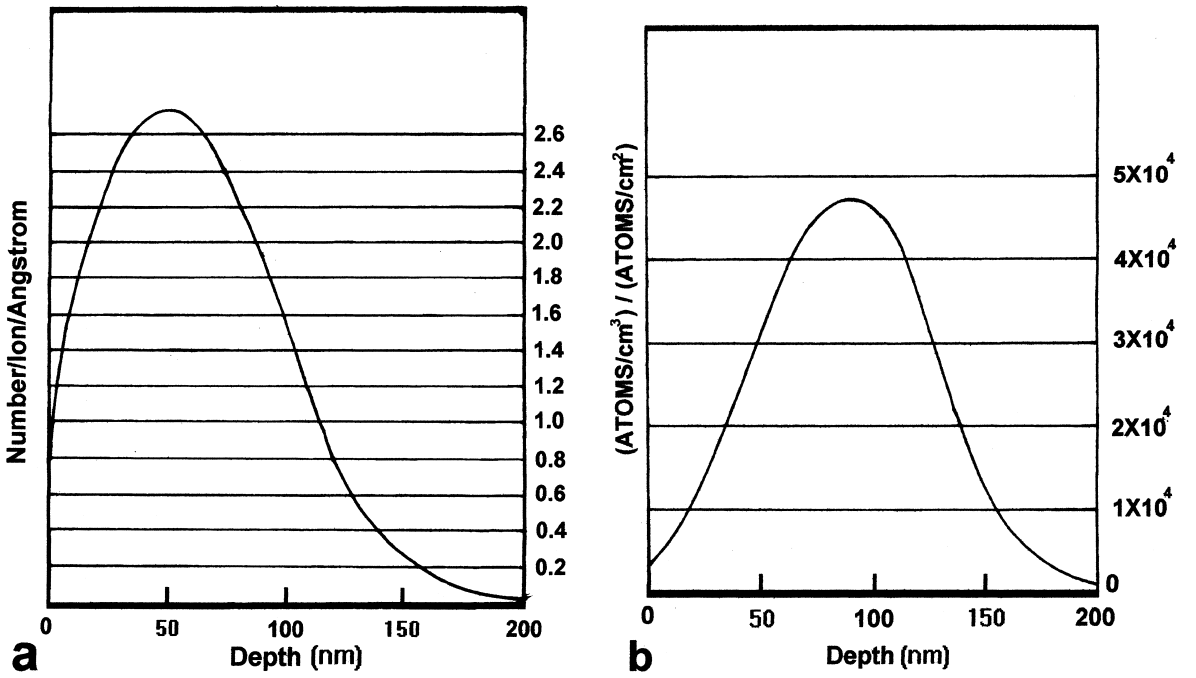

Fig. 5. The computer simulation with the TRIM code: (a) The vacancy distribution along the depth in the specimen by 300 keV Cu^+ ions; (b) The distribution of incident ions along the depth.

5. Conclusions

The Cu–Al25 alloy was irradiated by 300 keV Cu^+ ions at room temperature.

The TEM observations show that:

- When the specimens are irradiated to 10 dpa, the small alumina particles (~4 nm in diameter) are dissolved. The dissolution of Al_2O_3 particles is enhanced with increasing fluences to 30 dpa.
- A large number of small Frank dislocation loops (~5 nm in diameter) with different a/3 ⟨1 1 1⟩ Burgers vectors are produced. Both vacancy and interstitial loops are observed.
- At the region adjacent to the irradiation surface the number of vacancy loops is more than that of interstitial ones. This result is in good agreement with the computer simulation results.

Acknowledgements

The authors would like to thank Prof. B.N. Singh, Prof. R.P. Wahi and Drs. N. Wanderka for supplying the Glidcop Al25 alloy, Prof. Ruyi Chen and Mr. Ji Xia for assistance with the ion irradiation, Mrs. Ying Yua for advice on TEM specimen preparation, Prof. Xiaofeng Duan for discussion on TEM technique.

References

[1] J.A. Spitznagel, N.J. Doyle, W.J. Choyke, J.G. Greggi Jr., J.N. Mcgruer, J.W. Davis, Nucl. Instr. and Meth. B 16 (1986) 279.
[2] H.R. Brager, J. Nucl. Mater. 141–143 (1986) 79.
[3] H.R. Brager, J. Nucl. Mater. 141–143 (1986) 163.
[4] R.J. Livak, T.G. Zocco, L.W. Hobbs, J. Nucl. Mater. 144 (1987) 121.
[5] N. Wanderka, Y. Yuan, L. Jiao, R.P. Wahi, H. Wollenberger, J. Nucl. Mater. 191–194 (1992) 1356.
[6] V.R. Barabash, A.A. Gervash, A.N. Naberenkov, E.V. Nesterova, V.V. Rybin, S.A. Fabritsiev, J. Nucl. Mater. 191–194 (1992) 411.
[7] S.J. Zinkle, A. Horsewell, B.N. Singh, W.F. Sommer, J. Nucl. Mater. 195 (1992) 11.
[8] M. Rühle, M. Wilkens, U. Essmann, Phys. Stat. Sol. 11 (1965) 819.
[9] M. Rühle, Phys. Stat. Sol. 19 (1967) 263.
[10] M. Rühle, Phys. Stat. Sol. 19 (1967) 279.
[11] H. Diepers, Phys. Stat. Sol. 24 (1967) 235.
[12] M. Wilkens, in: S. Amelinckx, R. Gevers, G. Remaut, J. Van Landuyt (Eds.), Material Science, North-Holland, Amsterdam, 1970, p. 233.
[13] J.W. Edington, Practical Electron Microscopy in Materials Science, Thomson Litho Ltd., East Kilbride, Scotland, vol. 3, 1975, p. 32.
[14] J.W. Edington, Practical Electron Microscopy in Materials Science, Thomson Litho Ltd., East Kilbride, Scotland, vol. 4, 1976, p. 6.
[15] J. Yu, Chinese J. Nucl. Sci. Eng. 9 (1989) 237; 336.